

Please cite this article in press as: Tan A, Wehr M, Balanced tone-evoked synaptic excitation and inhibition in mouse auditory cortex, *Neuroscience* (2009), doi: 10.1016/j.neuroscience.2009.07.032

Neuroscience xx (2009) xxx

BALANCED TONE-EVOKED SYNAPTIC EXCITATION AND INHIBITION IN MOUSE AUDITORY CORTEX

A. TAN AND M. WEHR*

Institute of Neuroscience, University of Oregon, Eugene, OR 97403, USA

Abstract—The recent characterization of excitatory and inhibitory synaptic receptive fields in rat auditory cortex laid the basis for further investigation of the roles of synaptic excitation and inhibition in cortical computation and plasticity. The mouse is an increasingly important model system because of the wide range of genetic tools available for it. Here we present the first *in vivo* whole-cell voltage-clamp measurements of synaptic excitation and inhibition in the mouse cortex. We find that a substantial population of auditory cortical neurons receives balanced synaptic excitation and inhibition, whose amplitude ratios and relative time courses remain approximately constant across tone frequency. We conclude that the synaptic mechanisms underlying tone-evoked auditory cortical responses in mice closely resemble those in rats, supporting the mouse as a suitable model for synaptic processing in auditory cortex. © 2009 IBRO. Published by Elsevier Ltd. All rights reserved.

Key words: *in vivo* whole-cell, voltage clamp, tonal receptive field, synaptic conductance.

Cortical computation is created by precise patterns of synaptic excitation and inhibition. These inputs sculpt sensory receptive fields, and are modulated to achieve cortical states appropriate to different behavioral contexts (Hensch and Fagiolini, 2004; Wang, 2008). Beginning with its decisive role in initiating the critical period, the proper regulation of excitation and inhibition continues to be crucial for adaptive, long-lasting, experience-dependent plastic changes throughout development and adulthood (Hensch, 2005; Hofer et al., 2006). Because these phenomena are well-established in auditory cortex, the neural circuitry of the auditory cortex may provide a framework for their common understanding (Weinberger, 2004; Ohl and Scheich, 2005).

Fundamental properties of auditory cortical receptive fields have been used to demonstrate the impact of environmental influences, behaviorally relevant sensory stimuli, and neuromodulators such as acetylcholine in models of dysfunction and its remediation (Zhang et al., 2001; Moucha and Kilgard, 2006; Tallal and Gaab, 2006). Synaptic excitation and inhibition have distinctive roles in these models. In early development, environmental noise not only delays critical period closing, but also reduces the number of inhibitory neurons (de Villiers-Sidani et al.,

2008). In adult rats, tone-evoked synaptic excitation and inhibition were recently shown by *in vivo* whole-cell measurements to be typically ‘balanced’, with approximately constant amplitude ratios and time courses across different stimuli (Wehr and Zador, 2003; Zhang et al., 2003). Interestingly, this balance of excitation and inhibition is perturbed after acoustic trauma (Scholl and Wehr, 2008) and during cholinergic plasticity (Froemke et al., 2007).

Powerful genetic tools can be deployed to investigate these models if the key phenomena are established in the mouse (Luo et al., 2008). For example, the characterization of visual cortical plasticity in the mouse allowed the elucidation of excitatory and inhibitory circuitry via such methods (Gordon and Stryker, 1996; Hensch et al., 1998; Hensch, 2005). In addition, mouse models may permit *in vivo* and *in vitro* data to be closely integrated through the use of thalamocortical slice preparations (Agmon and Connors, 1991; Cruikshank et al., 2002; MacLean et al., 2006). Mice share fundamental auditory cortical receptive field and cholinergic plasticity properties with other mammals (Stiebler et al., 1997; Shen et al., 1999; Linden et al., 2003), but the extent of the similarity at the synaptic level remains unclear. Here we present the first *in vivo* whole-cell voltage-clamp measurements of synaptic excitation and inhibition in the mouse cortex. We find that in mice, as in rats, a substantial population of auditory cortical neurons receives balanced tone-evoked synaptic excitation and inhibition. The presence of this phenomenon in the mouse may facilitate its use for understanding cortical function.

EXPERIMENTAL PROCEDURES

All procedures were approved by the University of Oregon Animal Care and Use Committee, and minimized discomfort and the number of animals used. The 24 neurons whose tonal receptive fields (TRFs) are described in this report are from 20 mice. In most of these mice, we obtained only one whole-cell recording that met our conditions for recording quality, although in a few mice we obtained two to three recordings. We attempted recordings in a total of 112 mice.

Physiological procedures

Physiological procedures were based on those previously described (Stiebler et al., 1997; Arras et al., 2001; Linden et al., 2003). We used C57BL/6 mice of age 4–32 weeks (for current clamp recordings) or 4–12 weeks (for voltage-clamp recordings). Mice were anesthetized with 120–180 mg/kg ketamine, 0.24–0.36 mg/kg medetomidine, and 0–4.5 mg/kg acepromazine, by i.p. injection; the dose was adjusted to eliminate the pedal withdrawal reflex. Additional i.p. injections (20–80 mg/kg ketamine, 0.04–0.16 mg/kg medetomidine) were administered as necessary throughout the rest of the experiment. Dilute 0.1%–0.5% lidocaine, not exceeding 5 mg/kg, was topically applied at all points at which pressure was to be applied or incisions made. Respiratory

*Corresponding author. Tel: +1-541-346-5866.

E-mail address: wehr@uoregon.edu (M. Wehr).

Abbreviations: CF, characteristic frequency; TRF, tonal receptive field.

tract secretions and brain swelling were reduced by i.p. injection of 0.25 mg/kg atropine sulfate and 20 mg/kg dexamethasone. Each mouse was placed on a homeothermic heating pad which kept its temperature at 37 °C. The head was held fixed by a custom-made device that clamped it at both orbits and the palate, leaving the ears unobstructed. A cisternal drain was performed. The left auditory cortex was exposed by retracting the skin and muscle overlying it, followed by a craniotomy and a durotomy. The cortical surface was covered with 4% agarose in saline (0.9% NaCl), and kept moist with saline. In order to locate well-tuned regions of auditory cortex, we obtained a coarse map using local field potential recordings obtained 300–400 μm below the cortical surface with 5–7 M Ω patch pipettes containing saline.

Whole-cell recordings

Standard blind *in vivo* whole-cell recordings were obtained as previously described (Margrie et al., 2002; Wehr and Zador, 2003). For a reference electrode we inserted a silver-silver chloride wire into muscle near the base of the skull, and covered it with 4% agarose in saline to reduce changes in the surrounding fluid and concomitant changes in associated junction potentials. We assumed the potential of the cerebrospinal fluid to be uniform and equal to that of the reference electrode. We used 5–7 M Ω pipettes

to record from neurons 250–650 μm below the cortical surface (as determined by micromanipulator travel, corrected for angle of insertion). For recordings employing only current clamp, pipettes contained (in mM) 120 K-gluconate, 2 MgCl₂, 0.05 CaCl₂, 10 BAPTA, 4 MgATP, 10 phosphocreatine (2Na), and 10 HEPES, pH adjusted to 7.3 with KOH (Sigma Aldrich, MO, USA). For recordings employing only voltage clamp or both voltage and current clamp, pipettes contained (in mM) 1 QX-314, 130 Cs-methanesulfonate, 4 TEA-Cl, 0.5 BAPTA, 4 MgATP, 10 phosphocreatine (2Na), and 10 HEPES, pH 7.3 with CsOH (Sigma Aldrich, MO, USA). Based on preliminary observations (data not included in this report), we suspect that the use of 6 mM QX-314 in the internal solution may reduce mouse auditory cortical responsiveness over the course of a few hours. Although QX-314 acts intracellularly and is largely membrane impermeable, its extracellular accumulation has been reported to reduce spiking after a sufficient amount of time in guinea-pig cortical slice (Connors and Prince, 1982). We minimized accumulation of QX-314 in the cerebrospinal fluid during voltage-clamp experiments by using a relatively low concentration (1 mM) of QX-314 in the pipette, and by elevating pressure in the pipette only as much as needed to prevent its tip from clogging. Current and voltage clamping were carried out with an Axopatch 200 B patch-clamp amplifier (Molecular Devices,

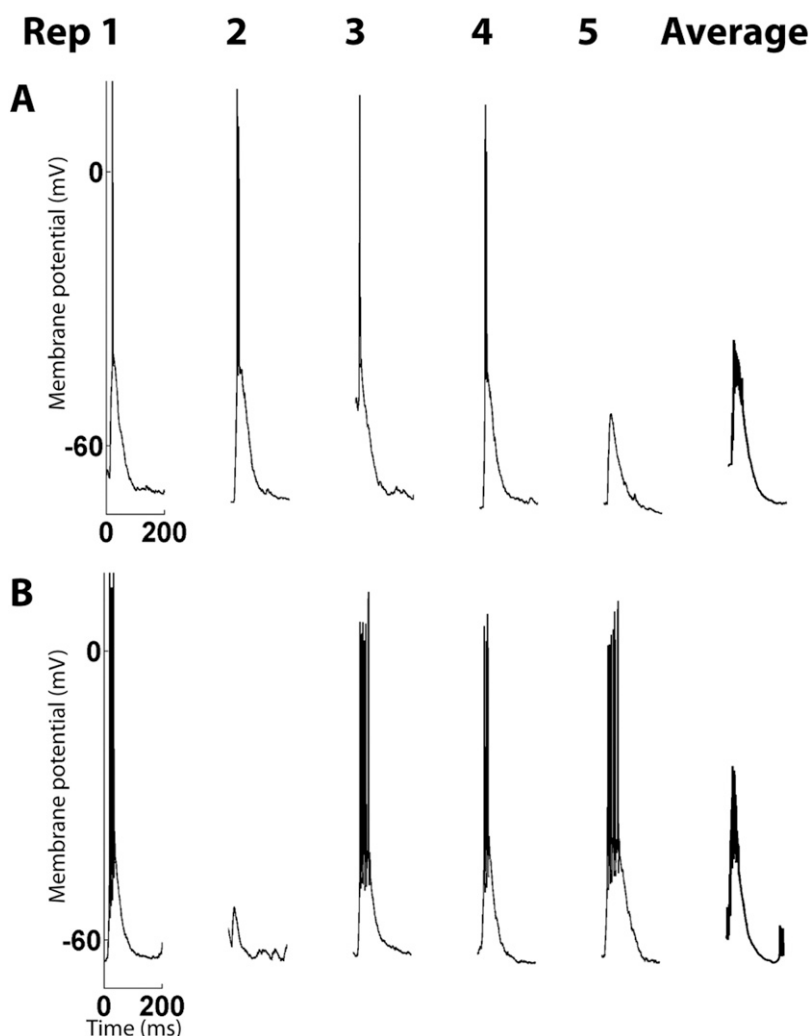


Fig. 1. Best frequency tone-evoked membrane potential responses. A (6 kHz, 60 dB) and B (6 kHz, 60 dB) are from different neurons. Each row shows five responses and their average. Tone onset 0 ms, tone duration 25 ms, in this and subsequent figures.

CA, USA). In recordings with the potassium-based pipette solution, resting membrane potentials ranged from -50 to -70 mV; we did not correct for the liquid junction potential. In recordings with the cesium-based pipette solution, resting membrane potentials ranged from -10 to -40 mV; when recording membrane potential responses we injected constant current to hyperpolarize the membrane potential (in the absence of a tone) to -60 to -80 mV; we corrected for a calculated liquid junction potential of 10 mV. Input or effective leak resistances ranged from 30 to 130 M Ω . Series resistances ranged from 30 to 100 M Ω for current clamp recordings, and 30–60 M Ω for voltage-clamp recordings.

Stimuli

Experiments were carried out in a sound isolation booth. Stimuli were pure tone pips delivered by a calibrated free field speaker directed at the right ear. Each tone pip was 25 ms long, with 3 ms cosine-squared rising and falling phases. The interval between successive tone onsets was 500 ms. We used two tone arrays: an isointensity tone array to rapidly characterize frequency tuning at 60 dB, and a full tone array with eight intensities to completely characterize frequency-intensity tuning. The isointensity tone array consisted of 15 logarithmically-spaced frequencies (3/octave) spanning 1.5–38.1 kHz, with intensity 60 dB SPL. The full tone

array consisted of 120 tones, at 15 logarithmically-spaced frequencies (3/octave) spanning 1.5–38.1 kHz, and eight tone intensities spanning 0–70 dB SPL in 10 dB steps. For each stimulus set we presented several repetitions of each tone.

Analysis

Synaptic conductances were estimated from synaptic currents as previously described (Wehr and Zador, 2003). The excitatory synaptic conductance $G_e(t)$ and inhibitory synaptic conductance $G_i(t)$ at time t were derived using

$$\Delta I(t, V) = G_e(t)(V - E_e) + G_i(t)(V - E_i) \quad (1)$$

where V is the membrane potential; E_e and E_i are the reversal potentials of the excitatory and inhibitory synaptic conductances, respectively; and $\Delta I(t, V)$ is the synaptic current, which is the difference between the total and leak currents at V . The values of E_e and E_i were 0 and -85 mV, respectively, as calculated from the ionic composition of the pipette solution and the cerebrospinal fluid; $G_e(t)$ and $G_i(t)$ were the two unknowns in Equation 1 at any particular t . Measurement of $\Delta I(t, V)$ at two different values of V yielded a system of two equations that could be solved for $G_e(t)$ and $G_i(t)$ at any particular t . Currents into the neuron were as-

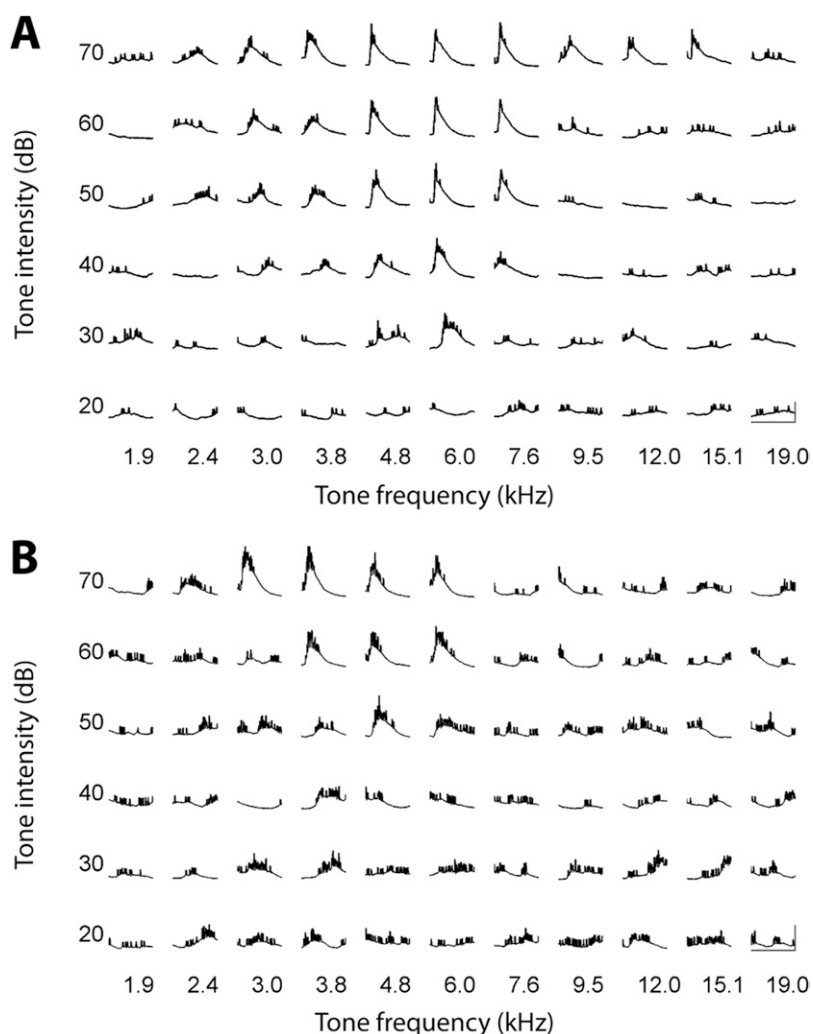


Fig. 2. TRFs of mean membrane potential responses. A and B are the neurons of Fig. 1A, 1B respectively. Horizontal scale bars=150 ms; vertical scale bars=20 mV.

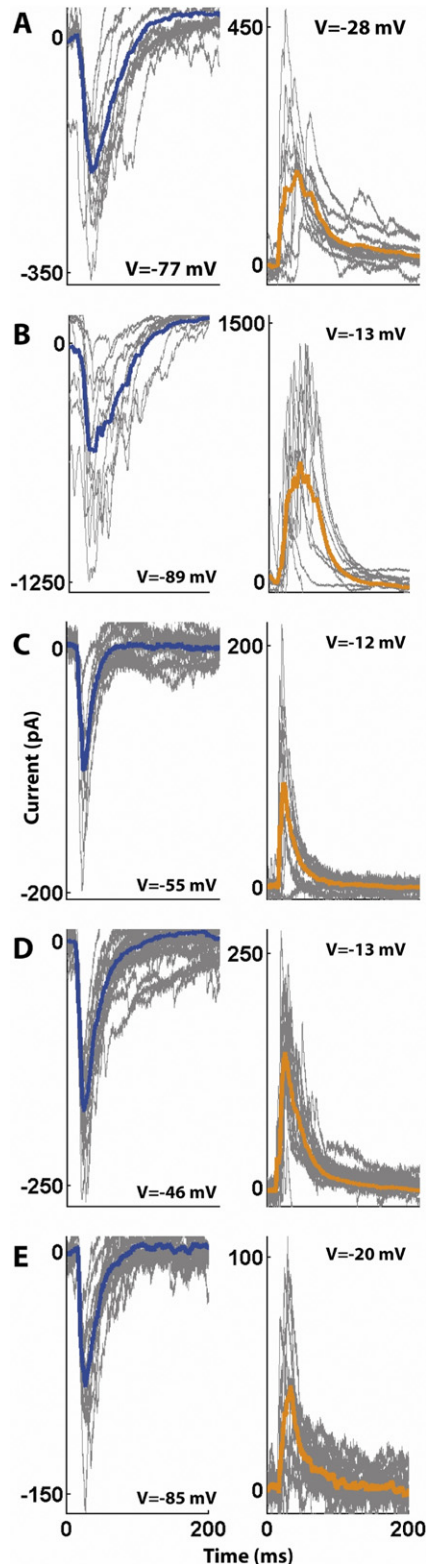


Fig. 3. Best frequency tone-evoked synaptic currents. A–E are each from a different neuron. Left panels: five superimposed currents (gray) and their average (blue) at a holding potential near the inhibitory potential ($V = -77, -89, -55$ mV, -46 , and -85 mV). Right panels: five superimposed currents (gray) and their average (orange) at a potential

signed a negative value. The membrane potential V was approximated as $V = V_c - R_s I(t, V_c)$, where V_c was the command potential, R_s the series resistance, and $I(t, V_c)$ the total current at V_c .

The excitatory and inhibitory synaptic conductances $G_e(t)$ and $G_i(t)$ were used to obtain the predicted membrane potential $V_p(t)$ by numerical integration of

$$C \frac{dV_p}{dt} = -G_e(t)(V - E_e) - G_i(t)(V - E_i) - G_o(V - E_o) \quad (2)$$

where C is the membrane capacitance, G_o is the leak conductance, and E_o is the membrane potential in the absence of a tone; C and G_o were estimated from current responses to voltage steps; E_o was set to -70 mV or taken from actual membrane potential responses if they were recorded.

Latency analyses for 60 dB tones (Figs. 4–8, 10–11, Table 1 Neurons 1–11) included synaptic conductances at all tone frequencies between and including the lowest and highest tone frequencies at which both the peak excitatory and inhibitory current exceeded two standard deviations of the leak current. There were essentially no responses to frequencies outside that bandwidth. Analyses of peak values also included three consecutive tone frequencies below and above that bandwidth, provided they were within the tone array. The criterion for inclusion in the peak analyses was slightly broader than that for the latency analyses, because a non-response can be assigned a well-defined amplitude (zero), but not a well-defined latency.

Analyses with the full tone array (Fig. 9, Table 1 Neuron 12) included synaptic conductances at all tone frequencies and intensities at which both peak excitatory and inhibitory current exceeded two standard deviations of the leak current; the resulting response area was not strictly contiguous in frequency and intensity, but was dominated by a contiguous V-shaped area apparent to visual inspection. Analyses of peak values also included all tone frequencies 10 dB below the threshold tone intensity.

Suppose a neuron exhibits a small response to a frequency just outside its responsive bandwidth (as defined above) that is mostly inhibition or mostly excitation. According to the above criteria, the frequency would not be included in analyses of latencies; however, because it would be included in the analyses of peak values, such a deviation from balance would still be detected by our analyses. For both tone arrays, analyses of peak values and latencies were restricted to the first 100 ms after tone onset. Fig. 10 includes only relative frequencies (distances from best frequency) for which there were responses within the bandwidth from at least two neurons so that a standard error could be obtained. Fig. 11 excludes one data point at -64 ms to present the data at a scale needed for visual clarity; however, that data point was included in all statistical analyses.

RESULTS

We obtained whole-cell recordings from a region of the left auditory cortex whose tone-evoked local field potentials formed a ‘V-shaped’ or ‘single-peaked’ response area, defined as a response area that was contiguous in tone frequency and intensity with a definable characteristic frequency (CF), being less than one octave wide near minimum threshold intensity, and broader at higher intensities. CF was the mean frequency at which membrane potential or current responses could be evoked at the minimum threshold intensity. Tone-evoked membrane potential re-

V nearer the excitatory reversal potential ($V = -28, -13, -12$ mV, -13 , and -20 mV). For interpretation of the references to color in this figure legend, the reader is referred to the Web version of this article.

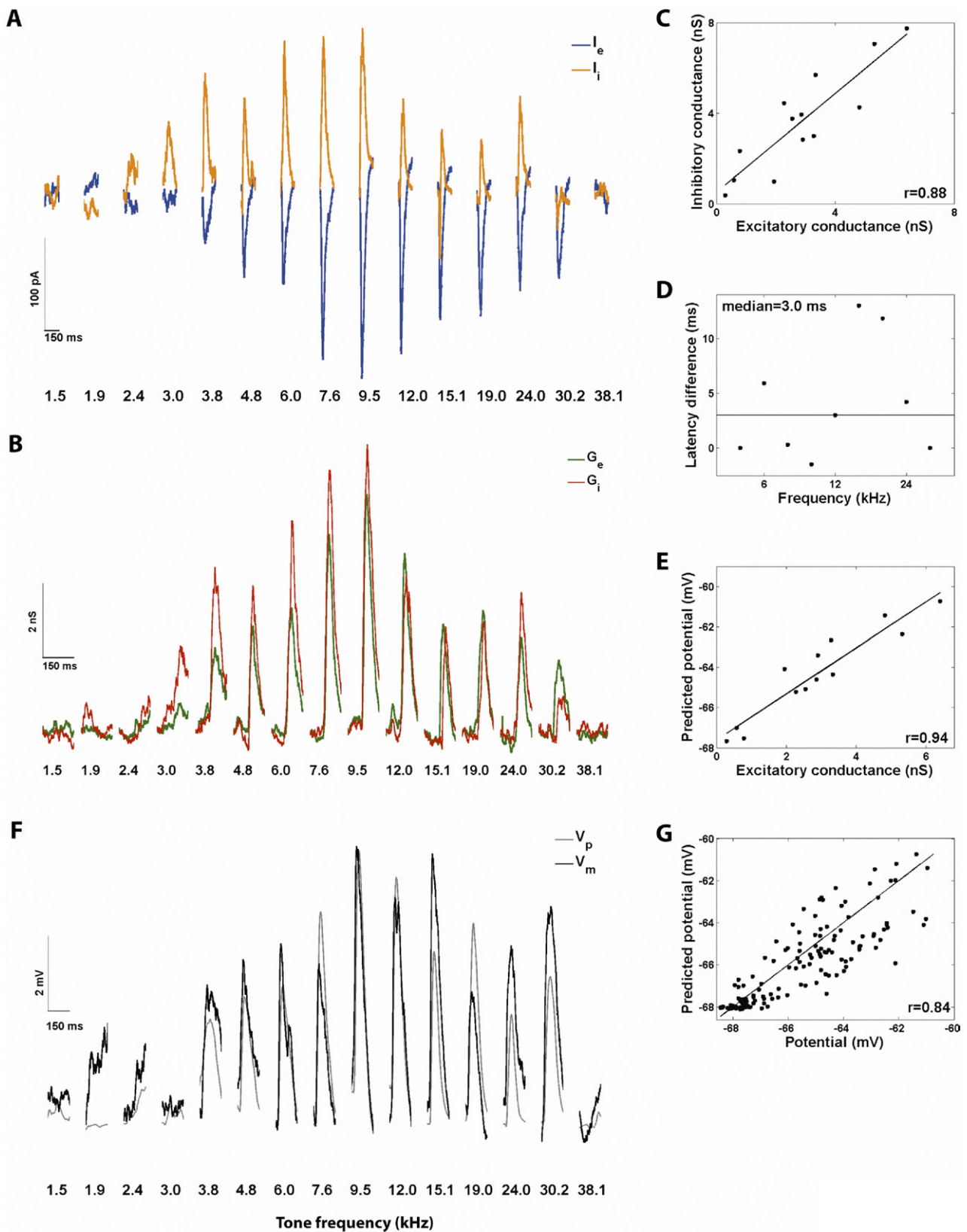
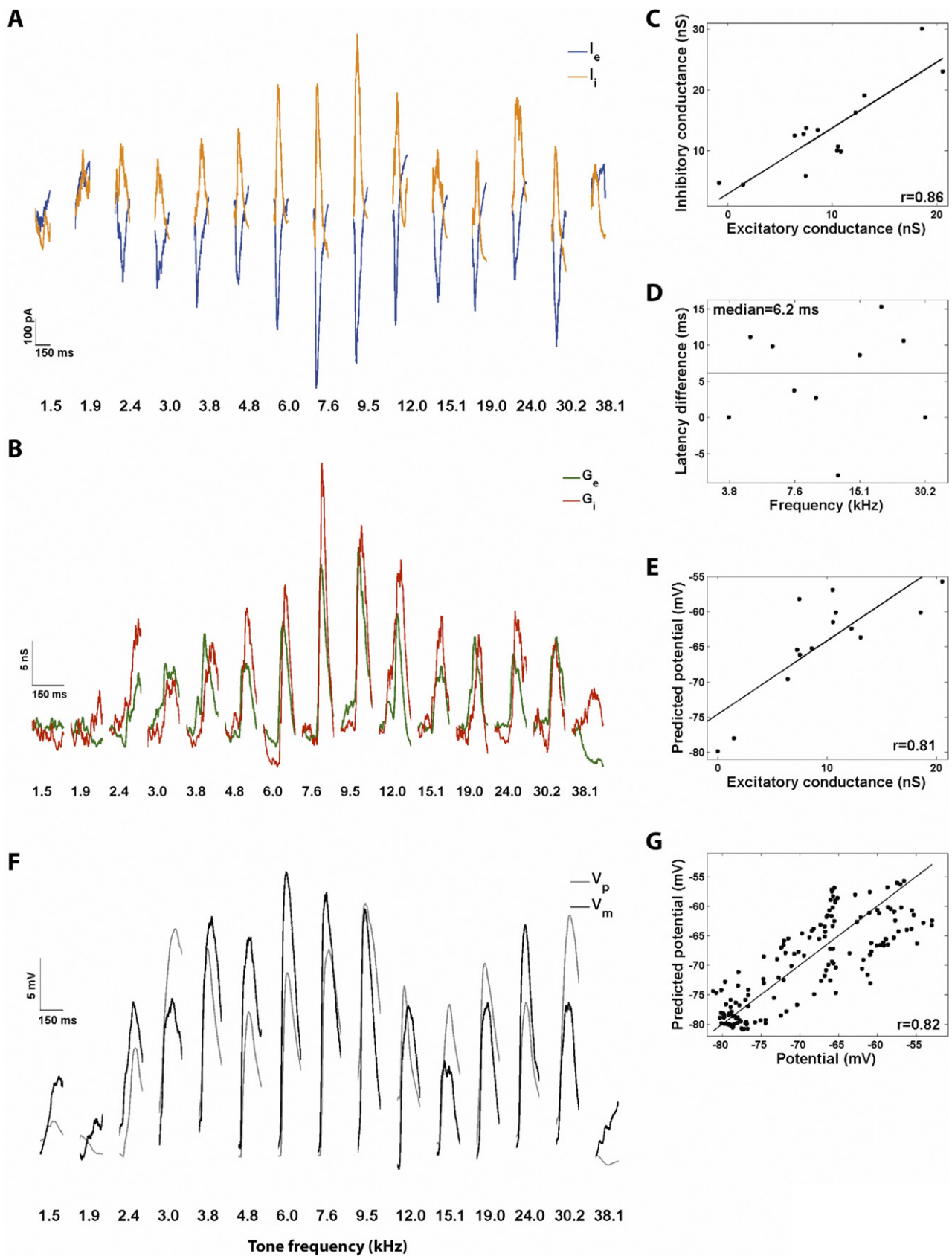


Fig. 4. Balanced tone-evoked synaptic excitation and inhibition. Same neuron as Fig. 3A. (A) Frequency tuning at 60 dB of excitatory (blue) and inhibitory (orange) currents. (B) Frequency tuning at 60 dB of excitatory (green) and inhibitory (red) conductances. (C) Peak inhibitory conductance versus peak excitatory conductance; line indicates linear regression. (D) Latency difference between inhibitory conductance and excitatory conductance as a function of frequency; horizontal line indicates median. (E) Peak predicted membrane potential versus peak excitatory conductance; line indicates linear regression. (F) Frequency tuning at 60 dB of predicted (gray) and actual (black) membrane potential responses. (G) Predicted versus actual membrane potential responses; line indicates unity slope. For interpretation of the references to color in this figure legend, the reader is referred to the Web version of this article.



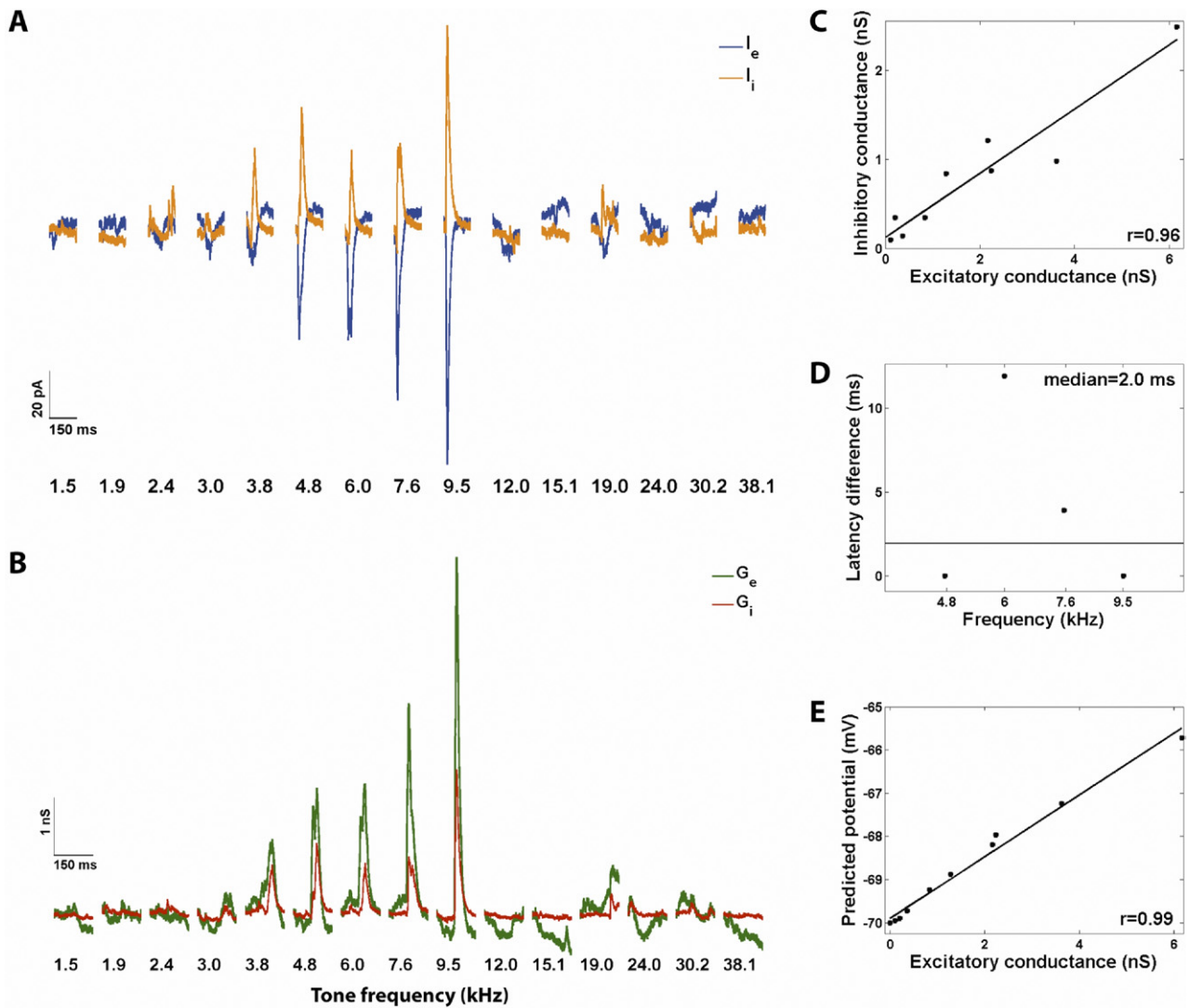


Fig. 6. Balanced tone-evoked synaptic excitation and inhibition. Same neuron as Fig. 3C. (A) Frequency tuning at 60 dB of excitatory (blue) and inhibitory (orange) currents. (B) Frequency tuning at 60 dB of excitatory (green) and inhibitory (red) conductances. (C) Peak inhibitory conductance versus peak excitatory conductance. (D) Latency difference between inhibitory conductance and excitatory conductance as a function of frequency; horizontal line indicates median. (E) Peak predicted membrane potential versus peak excitatory conductance. For interpretation of the references to color in this figure legend, the reader is referred to the Web version of this article.

sponses measured by whole-cell current clamp recordings from single neurons in these regions had similarly V-shaped response areas, and we will begin by briefly describing them, as they provide some indication about the location of our recordings relative to the cortical fields defined by extracellular recordings (Linden et al., 2003; Shen et al., 1999; Stiebler et al., 1997). We will then turn our attention to whole-cell voltage-clamp estimates of the tone-evoked excitatory and inhibitory synaptic inputs received by single neurons in these regions.

Tone-evoked membrane potential responses

We obtained whole-cell current clamp recordings of tone-evoked membrane potential responses from 12 neurons, and characterized full TRFs in six neurons. Fig. 1A, B show typical tone-evoked membrane potential responses from two neurons. In both neurons, each of five repetitions of a 60 dB, CF tone evoked a brief depolarization which began approximately 15 ms after tone onset, and was largely over at 100 ms after tone onset. Four of the five depolarizations were

Fig. 5. Balanced tone-evoked synaptic excitation and inhibition. Same neuron as Fig. 3B. (A) Frequency tuning at 60 dB of excitatory (blue) and inhibitory (orange) currents. (B) Frequency tuning at 60 dB of excitatory (green) and inhibitory (red) conductances. (C) Peak inhibitory conductance versus peak excitatory conductance. (D) Latency difference between inhibitory conductance and excitatory conductance as a function of frequency; horizontal line indicates median. (E) Peak predicted membrane potential versus peak excitatory conductance. (F) Frequency tuning at 60 dB of predicted (gray) and actual (black) membrane potential responses. (G) Predicted versus actual membrane potential responses. For interpretation of the references to color in this figure legend, the reader is referred to the Web version of this article.

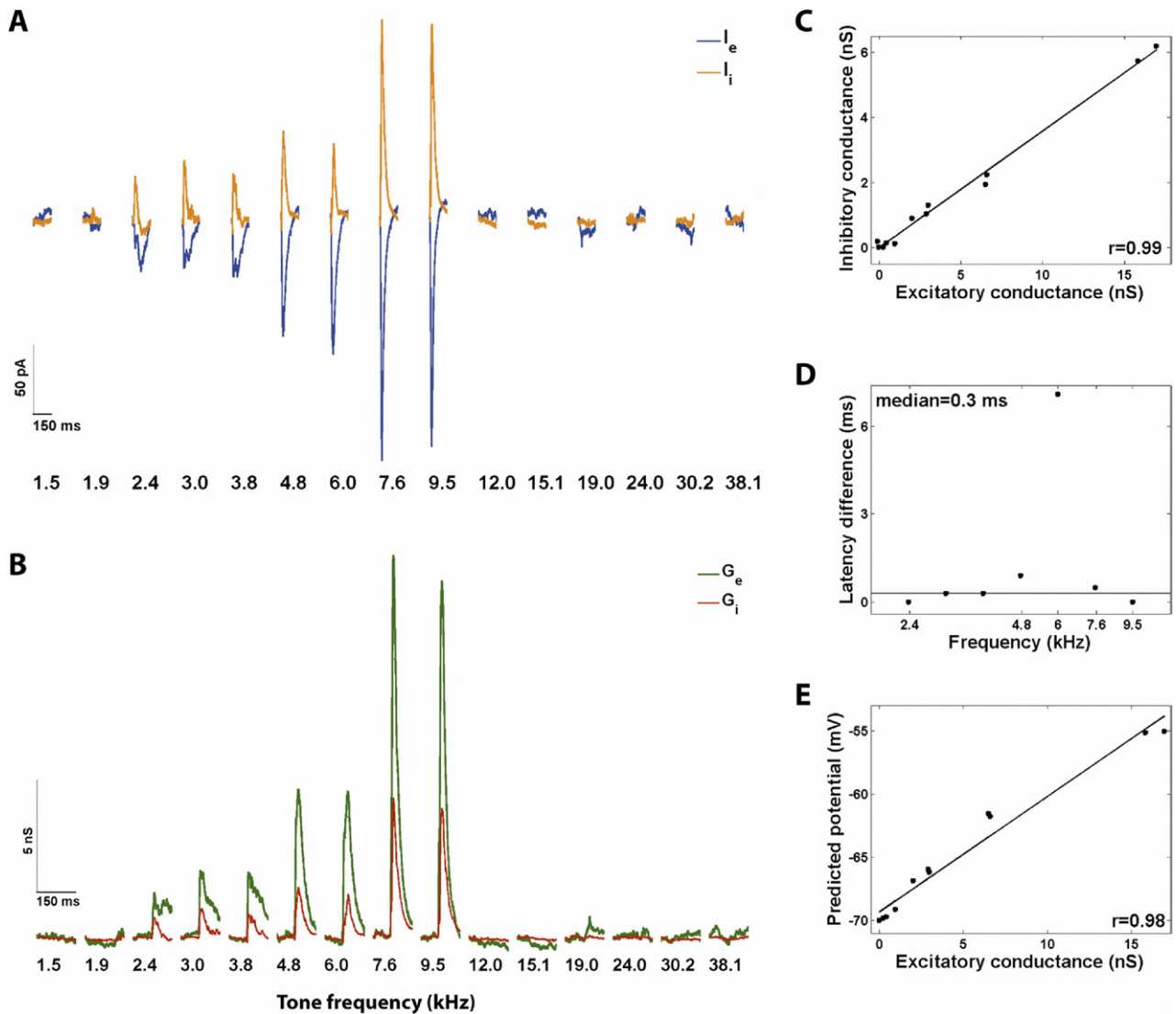


Fig. 7. Balanced tone-evoked synaptic excitation and inhibition. Same neuron as Fig. 3D. (A) Frequency tuning at 60 dB of excitatory (blue) and inhibitory (orange) currents. (B) Frequency tuning at 60 dB of excitatory (green) and inhibitory (red) conductances. (C) Peak inhibitory conductance versus peak excitatory conductance. (D) Latency difference between inhibitory conductance and excitatory conductance as a function of frequency; horizontal line indicates median. (E) Peak predicted membrane potential versus peak excitatory conductance. For interpretation of the references to color in this figure legend, the reader is referred to the Web version of this article.

large enough to evoke one or several spikes. In all 12 neurons, the trial-averaged response to a 60 dB tone at CF began 10–30 ms after tone onset and was largely over by 100 ms after tone onset. Bandwidth at 60 dB was 2.2 ± 1.0 octaves (mean \pm SD, $n=12$).

Fig. 2A, B show the respective TRFs of the averaged responses of the neurons of Fig. 1A, B. Neither neuron responded at the lowest tone intensity, regardless of tone frequency. At the threshold tone intensity (30 and 50 dB for the neurons of Fig 2A, B respectively), both neurons responded only to a narrow range of tone frequencies centered at the CF (6.0 and 4.8 kHz, respectively). As tone intensity increased, the neurons responded to broader frequency ranges. Each of their frequency-intensity response areas thus resembled an upright 'V' whose tip lay at threshold intensity and CF. All six neurons from which

full TRFs were obtained had V-shaped tuning curves. This suggests that our recordings were obtained either from the primary auditory field (AI), the anterior auditory field (AAF), or single peaked regions of the secondary auditory field (AII), but not the dorsoposterior field (DP); they were also probably not from the ultrasonic field (UF), because CFs were less than 38.1 kHz, the highest tone frequency that we presented; but the latter possibility cannot be excluded because many UF neurons are multip peaked with a significant peak within the range of frequencies we presented (Linden et al., 2003; Shen et al., 1999; Stiebler et al., 1997).

Tone-evoked synaptic excitation and inhibition

We used whole-cell voltage-clamp recordings of synaptic current responses to estimate the excitatory and inhibitory

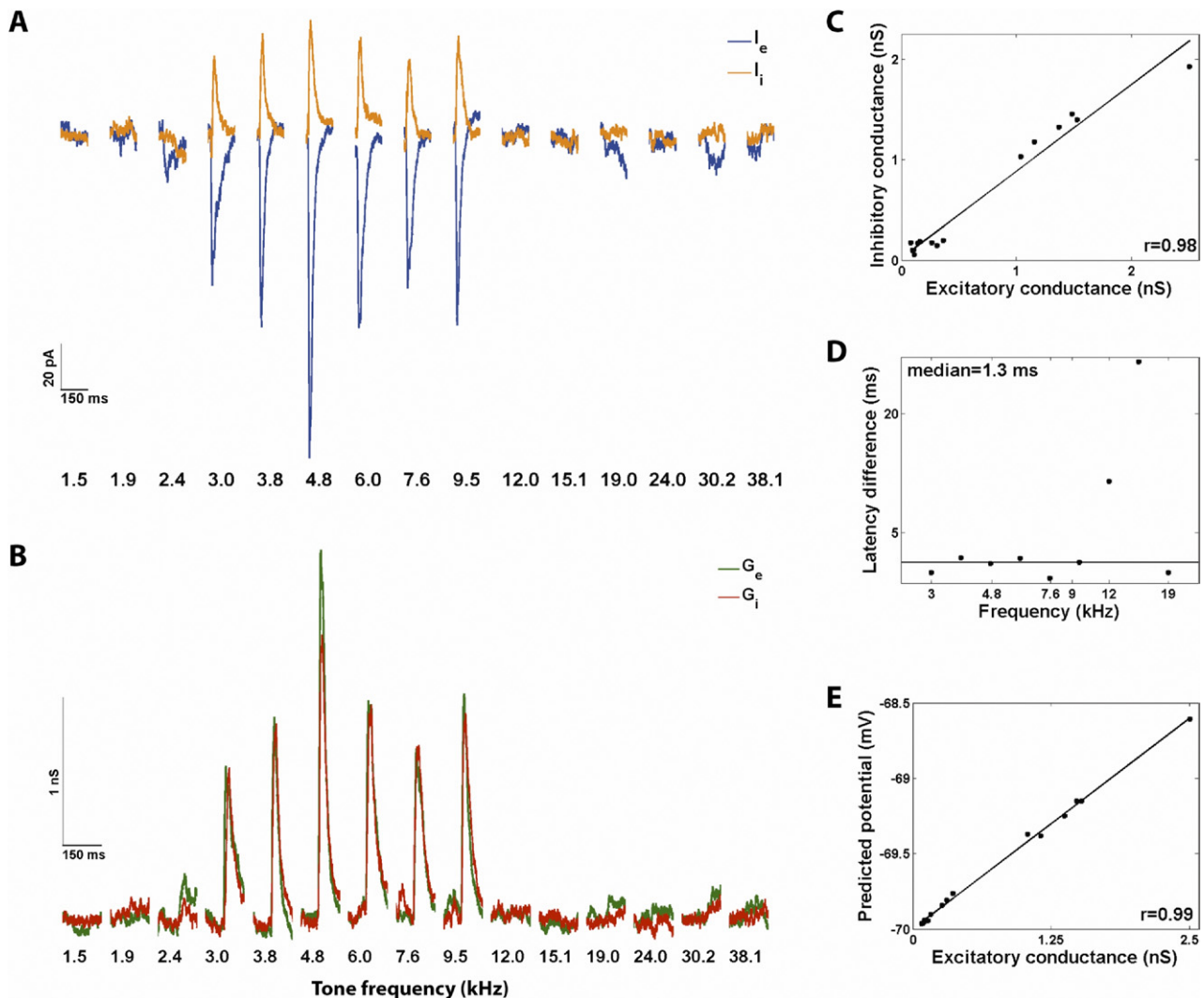


Fig. 8. Balanced tone-evoked synaptic excitation and inhibition. Same neuron as Fig. 3E. (A) Frequency tuning at 60 dB of excitatory (blue) and inhibitory (orange) currents. (B) Frequency tuning at 60 dB of excitatory (green) and inhibitory (red) conductances. (C) Peak inhibitory conductance versus peak excitatory conductance. (D) Latency difference between inhibitory conductance and excitatory conductance as a function of frequency; horizontal line indicates median. (E) Peak predicted membrane potential versus peak excitatory conductance. For interpretation of the references to color in this figure legend, the reader is referred to the Web version of this article.

synaptic conductances underlying tone-evoked membrane potential responses in another 12 neurons. We used at least five repetitions of each tone frequency and/or intensity to obtain average synaptic currents. We characterized the frequency tuning of synaptic excitation and inhibition at 60 dB in 11 neurons, and characterized full TRFs in one neuron. Bandwidth at 60 dB was 2.7 ± 1.1 octaves (mean \pm SD, $n=12$).

The synaptic currents evoked by a 60 dB, best frequency tone in five neurons are shown in Fig. 3A–E respectively. In all five neurons, when we clamped the membrane potential near the inhibitory reversal potential (left panels), each of five tone repetitions evoked an inward, mainly excitatory current (gray traces). The trial-average (blue trace) resembled the individual currents, demonstrating the reliability of the responses. When we depolarized neurons to a membrane potential near the excitatory reversal potential (right panels), each of five tone repetitions

evoked an outward, mainly inhibitory current (gray traces). Again, the trial-average (orange trace) resembled the individual currents. In all 12 neurons, the trial-averaged excitatory and inhibitory currents evoked by a 60 dB, best-frequency tone began 10–30 ms after tone onset, and were largely over by 100 ms after tone onset. The membrane potential responses and synaptic currents we recorded were thus reliable and had greatly overlapping ranges of response onset times and durations.

In the following, we have assumed that the trial-averaged excitatory and inhibitory synaptic currents resembled the corresponding currents on individual trials sufficiently for us to estimate conductances by comparing synaptic currents recorded at different membrane potentials, and hence during different tone presentations. Below we present evidence suggesting that this and other assumptions underlying the conductance estimations are reasonable.

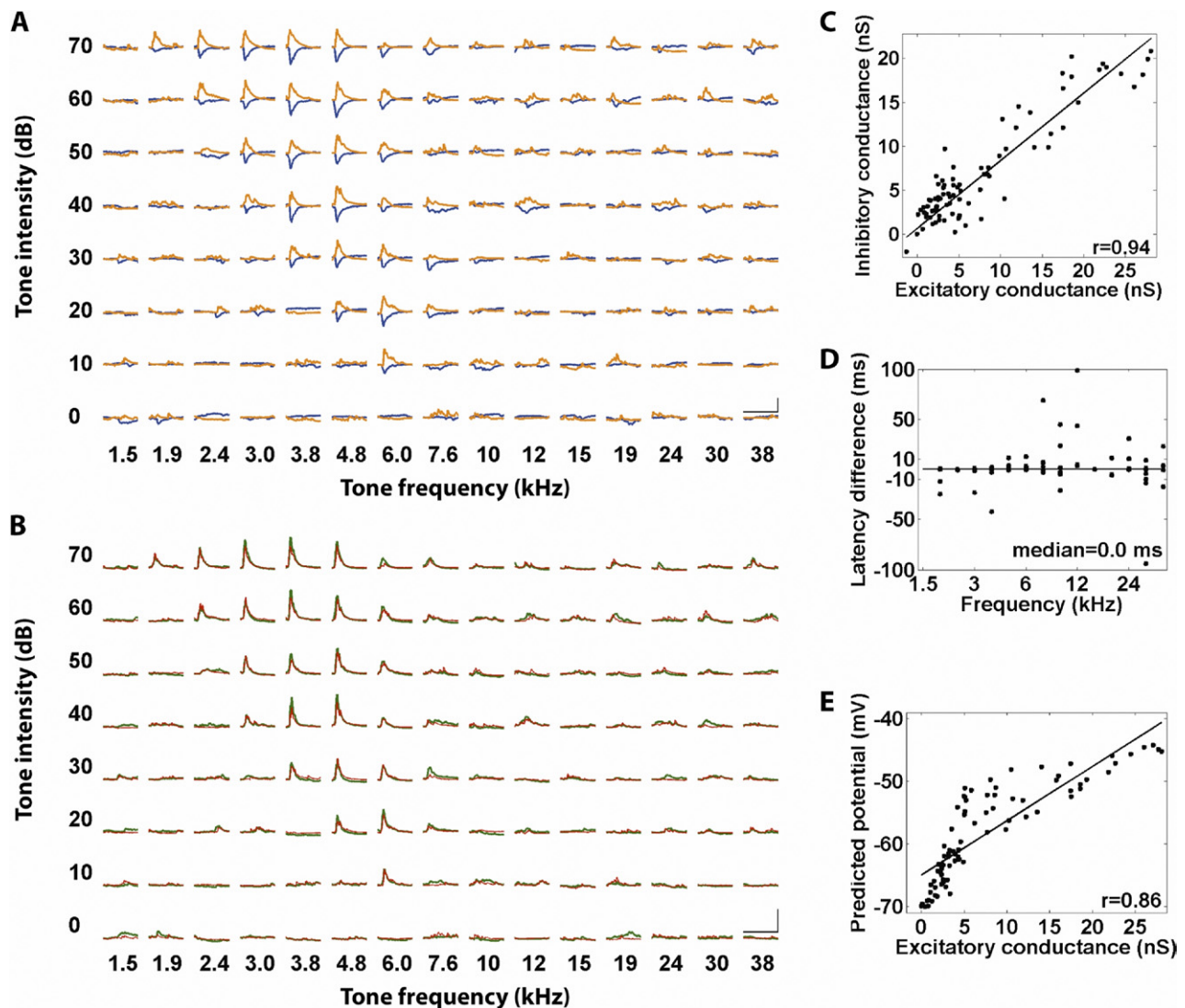


Fig. 9. Balanced tone-evoked synaptic excitation in an example neuron. (A) Tonal receptive field of excitatory (blue) and inhibitory (orange) currents. (B) Tonal receptive field of excitatory (green) and inhibitory (red) conductances. (C) Peak inhibitory conductance versus peak excitatory conductance. (D) Latency difference between inhibitory conductance and excitatory conductance as a function of frequency. (E) Peak predicted membrane potential versus peak excitatory conductance. Horizontal scale bars=150 ms (A). Vertical scale bars=400 pA (A), 20 nS (B). For interpretation of the references to color in this figure legend, the reader is referred to the Web version of this article.

Balanced synaptic excitation and inhibition in an example neuron

We now turn our attention to the frequency tuning of synaptic currents and conductances. We first examine the neuron shown in Fig. 4 (same neuron as Fig. 3A). Fig. 4A shows the inward, mainly excitatory currents (blue) and outward, mainly inhibitory currents (orange) evoked by 60 dB tones ranging from 1.5 to 38.1 kHz. The excitatory currents were frequency tuned to a contiguous range of tone frequencies from 3.0 to 30.2 kHz, with the largest current at the best tone frequency of 9.5 kHz. The frequency tuning and time course of the inhibitory currents were very similar to the excitatory currents, that is, the excitatory and inhibitory synaptic currents appear to be balanced.

To quantitatively assess the balance of excitation and inhibition, we estimated excitatory and inhibitory synaptic conductances from the synaptic currents with the further assumption of a single compartment model of the neuron. Analysis of conductances offers two advantages over analysis of the raw synaptic currents. First, a mainly excitatory current almost certainly still contains a small inhibitory component, because the membrane potential is unlikely to be clamped at exactly the inhibitory reversal potential. Thus the relative amplitudes of the excitatory and inhibitory currents need not reflect the frequency tuning of the relative amplitudes of the excitatory and inhibitory synaptic conductances if they are unbalanced. Second, the conductance estimates explicitly incorporate the most common assumptions that might be used to interpret the synaptic

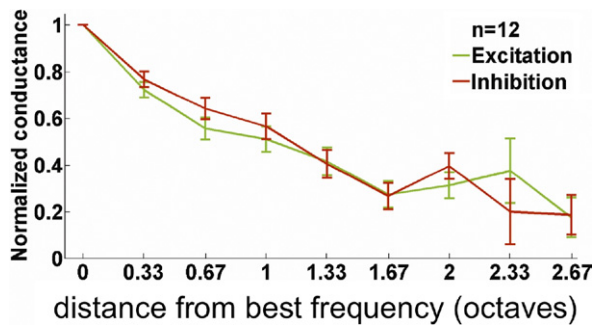


Fig. 10. Balanced tone-evoked synaptic excitation and inhibition in the population of neurons. Peak excitatory and inhibitory conductance versus magnitude of tone frequency difference from best tone frequency, mean \pm SEM across 12 neurons at 60 dB. For interpretation of the references to color in this figure legend, the reader is referred to the Web version of this article.

currents. Therefore, comparing the membrane potential responses predicted by the conductances against actual membrane potential responses can clarify the propriety of a straightforward interpretation of the currents.

Fig. 4B shows the excitatory (green) and inhibitory (red) synaptic conductances estimated from the currents of Fig. 4A. The conductances had the same salient features as the currents. The excitatory and inhibitory conductances were similarly tuned to a contiguous range of tone frequencies from 3.0 to 30.2 kHz, with a best frequency of 9.5 kHz. Fig. 4C shows that the peak values of the excitatory and inhibitory conductances were highly correlated (correlation coefficient $r=0.88$), demonstrating that the ratio of their amplitudes remained approximately constant across tone frequency.

To quantify the relative timings of the conductances, we defined 'latency' as the time after tone onset at which a conductance reached half its peak value. Fig. 4D shows the latency differences between the excitatory and inhibitory conductances were small (median: 3.0 ms) and did not vary systematically across their bandwidth. Thus the relative timing of excitation and inhibition also remained approximately constant across tone frequency.

If excitation and inhibition are perfectly balanced across all tone frequencies, the tuning of the membrane potential is essentially unchanged by inhibition, and will be similar to that of the excitatory conductance alone. Equivalently, the predicted membrane potential will be a monotonic function of the excitatory conductance. In contrast, if excitation and inhibition are unbalanced (for example, in a neuron for which inhibition enhances intensity tuning; Wu et al., 2006; Tan et al., 2007), the predicted membrane potential is a non-monotonic function of the excitatory conductance. Fig. 4E shows that, in this neuron, the peak value of the predicted membrane potential response was a monotonic function of the peak value of the excitatory conductance. In this neuron, therefore, the relative amplitudes and time courses of the excitatory and inhibitory conductances were sufficiently constant across tone frequency that the membrane potential tuning was essentially unchanged by inhibition. We conclude that excitation and inhibition were balanced in this neuron.

To test the linearity assumption underlying our conductance estimates, we recorded actual tone-evoked membrane potential responses in this neuron. In this way, we can compare the actual membrane potential responses to those predicted from our conductances (using Equation 2). Fig. 4F shows that the predicted (gray) and actual (black) membrane potential responses were similar; Fig. 4G shows that corresponding values of the predicted and actual membrane potential responses, taken at 10 ms intervals during the first 100 ms after tone onset, were highly correlated ($r=0.84$) and lay about a line of unity slope. This suggests that the linearity assumption underlying the conductance estimations were reasonable.

Balanced synaptic excitation and inhibition in the auditory cortex

We recorded membrane potential responses in addition to synaptic currents in one other neuron, shown in Fig. 5 (same neuron as Fig. 3B). Its excitatory and inhibitory currents and conductances had similar frequency tuning (Fig. 5A, B, C). The latency difference between excitatory and inhibitory conductances was approximately constant across tone frequency (Fig. 5D). The predicted membrane potential was a monotonic function of the excitatory conductance (Fig. 5E), indicating that inhibition did not substantially affect membrane potential tuning. The predicted

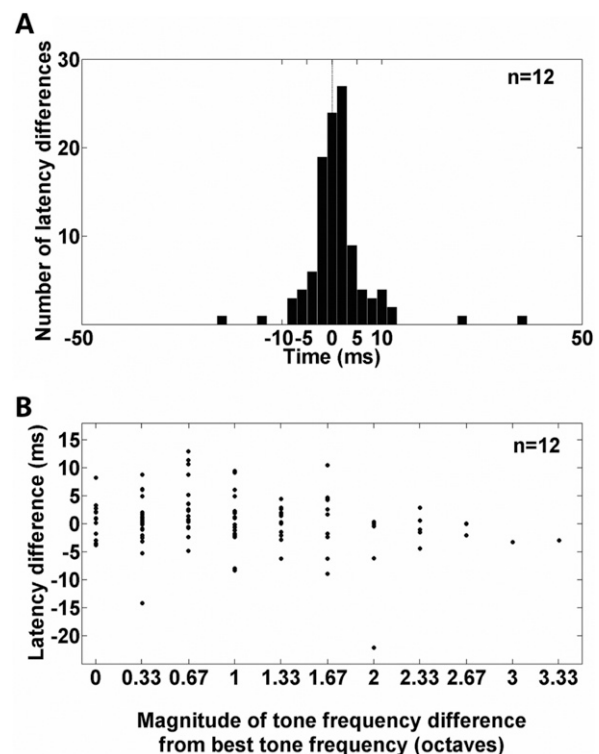


Fig. 11. Relative timing of excitatory and inhibitory conductances. (A) Histogram of the latency difference between excitatory and inhibitory conductances, across 12 neurons and all tone frequencies at 60 dB. (B) Latency difference between excitatory and inhibitory conductances versus magnitude of tone frequency difference from best tone frequency, across 12 neurons and all tone frequencies at 60 dB.

Table 1. Assessment of excitatory and inhibitory conductance balance

Neuron	Depth (μm)	Peak excitatory conductance vs. peak inhibitory conductance correlation coefficient (<i>P</i> -value)	Median latency difference (ms)	Latency difference vs. tone frequency correlation coefficient (<i>P</i> -value)	Peak predicted membrane potential response vs. peak excitatory conductance correlation coefficient (<i>P</i> -value)	Balanced?
1 (Fig.3)	625	0.88 (0.00)	3.0	0.28 (0.46)	0.94 (0.00)	Balanced
2 (Fig.4)	396	0.86 (0.00)	6.2	0.07 (0.84)	0.81 (0.00)	Balanced
3 (Fig.5)	430	0.96 (0.00)	2.0	0.18 (0.82)	0.99 (0.00)	Balanced
4 (Fig.6)	361	0.99 (0.00)	0.3	0.22 (0.64)	0.98 (0.00)	Balanced
5 (Fig.7)	284	0.98 (0.00)	1.3	0.48 (0.19)	0.99 (0.00)	Balanced
6 (Fig.8)	374	0.92 (0.00)	0.1	0.21 (0.73)	0.97 (0.00)	Balanced
7	286	0.98 (0.00)	0.7	0.36 (0.30)	0.99 (0.00)	Balanced
8	364	0.90 (0.00)	0.0	0.28 (0.35)	0.99 (0.00)	Balanced
9	423	0.68 (0.01)	-0.8	0.37 (0.17)	0.58 (0.02)	Less balanced
10	374	0.98 (0.00)	0.9	0.18 (0.58)	0.99 (0.00)	Balanced
11	414	0.97 (0.00)	-2.0	0.07 (0.85)	0.83 (0.00)	Balanced
12 (Fig.9)	491	0.94 (0.00)	0.0	0.21 (0.73)	0.86 (0.00)	Balanced

Responses were considered balanced if (1) Peak excitatory conductance was well correlated with peak inhibitory conductance with $P < 0.01$; (2) Latency difference was not significantly correlated with tone frequency; and (3) Peak predicted membrane potential response was well correlated with peak excitatory conductance with $P < 0.01$.

and actual membrane potential responses also matched reasonably well (Fig. 5F, G). We conclude that excitation and inhibition were also balanced in this neuron.

The remaining neurons of Fig. 3C–E are shown in Figs. 6–8 respectively, with traces and analyses displayed in the same format as in Figs. 4–5 (comparisons of predicted and membrane potentials are absent, because we did not record actual membrane potential responses in these neurons). Notably, the neurons of Figs. 4–8 displayed considerable variety in the bandwidths and asymmetries of their spectral profiles (Figs. 4–8, A–B), yet each was tuned to a contiguous range of tone frequencies, and received balanced excitatory and inhibitory synaptic input (Figs. 4–8, A–E). Moreover, the neuron for which we obtained full excitatory and inhibitory synaptic TRFs was balanced over its entire frequency-intensity response area (Fig 9).

As a group, all 12 neurons were balanced. Excitatory and inhibitory conductances at 60 dB were matched such that the ratio of their amplitudes remained approximately constant across tone frequency (Fig. 10). The latency difference between excitatory and inhibitory conductances at 60 dB was 0.7 ± 8.8 ms (mean \pm SD), and was distributed such that 77% were less than 5 ms (Fig. 11A); latency difference did not vary systematically with tone frequency (Fig. 11B). This latency difference of 0.7 ± 8.8 ms ($n = 12$) is not significantly different from that reported previously for rat auditory cortex (Wehr and Zador, 2003), which was 2.4 ± 3.6 ms ($n = 17$ for that sample, $t(27) = 0.72$, $P = 0.48$, independent sample t -test with pooled variance).

These descriptions were also individually appropriate for 11 of the 12 neurons (Table 1). Peak predicted membrane potential and peak excitatory conductance were well correlated in these 11 neurons, further indicating that the relative amplitudes and time courses of the excitatory and inhibitory conductances were sufficiently constant across tone frequency that the tuning of the membrane potential was essentially unchanged by synaptic inhibition (Table 1). We conclude that a substantial population of neurons in

the mouse auditory cortex receives balanced tone-evoked synaptic excitation and inhibition.

DISCUSSION

We have shown that balanced synaptic excitation and inhibition underlies tone-evoked responses of the mouse auditory cortex, as is the case in rats (Wehr and Zador, 2003; Zhang et al., 2003) and likely in cats (De Ribaupierre, 1972; Volkov and Galazjuk, 1991; Ojima and Murakami, 2002). Tone-evoked spiking responses of the mouse auditory cortex have also been shown to resemble those of other mammals in frequency tuning, time course, tonotopic organization and experience-dependent plasticity (Stiebler et al., 1997; Shen et al., 1999; Linden et al., 2003; Yan and Zhang, 2005). Our results provide a basis for the use of genetic tools to elucidate synaptic mechanisms of cortical function in mice (Liu, 2006).

In vitro experiments probe synaptic organization more directly than *in vivo* experiments, but the correspondence between neural activity *in vitro* and *in vivo* is poorly understood. *In vivo* whole-cell recordings can help to bridge this gap (Margrie et al., 2002; Tan and Borst, 2007). For example, our results provide an interpretation of mouse auditory thalamocortical slice data (Cruikshank et al., 2002; Rose and Metherate, 2005; Verbny et al., 2006; Kawai et al., 2007; Lee and Sherman, 2008; Oswald and Reyes, 2008), in which electrical stimulation of the thalamus or of cortical white matter produces depolarization that is followed by hyperpolarization at a delay of 1–6 ms (Cruikshank et al., 2002). This resembles the effect of tone stimulation *in vivo*, and suggests that electrical and tone stimulation produce similar patterns of neural activity (Figs. 1–9). Which electrical or optical stimulation parameters best correspond to varying tone frequency remains an interesting open question (Deisseroth et al., 2006; Nikolenko et al., 2007).

Balanced excitation and inhibition is consistent with individual presynaptic excitatory and inhibitory neurons being identically tuned. There are, however, populations of excitatory and inhibitory neurons in which the latter are more broadly tuned (Sohya et al., 2007; Atencio and Schreiner, 2008; Niell and Stryker, 2008). Measurements of synaptic receptive fields at a finer tone frequency resolution may therefore show subtle deviations from balance (Wu et al., 2008). In addition, tone-evoked inputs from excitatory and inhibitory neurons could differ in convergence and divergence (Watts and Thomson, 2005). It remains to be seen if more diverse patterns of synaptic input will be revealed in awake animals, or by complex sounds, or in auditory cortical regions with multi-peaked tuning curves (Sutter et al., 1999; Chechik et al., 2006). Synaptic excitation and inhibition in mouse auditory cortex are therefore likely to show subtle deviations from perfect balance, but this nevertheless provides an important constraint on circuit models of cortical function (Dominguez et al., 2006; Soto et al., 2006; Simon et al., 2007; de la Rocha et al., 2008).

Acknowledgments—We thank Ben Scholl for help with preliminary experiments; and Craig Atencio, Robert Froemke, Tomáš Hromádka, Hysell Oviedo, and William Roberts for discussions.

REFERENCES

- Agmon A, Connors BW (1991) Thalamocortical responses of mouse somatosensory (barrel) cortex *in vitro*. *Neuroscience* 41:365–379.
- Arras M, Autenried P, Rettich A, Spaeni D, Rüllicke T (2001) Optimization of intraperitoneal injection anesthesia in mice: drugs, dosages, adverse effects, and anesthesia depth. *Comp Med* 51:443–456.
- Atencio CA, Schreiner CE (2008) Spectrotemporal processing differences between auditory cortical fast-spiking and regular-spiking neurons. *J Neurosci* 28:3897–3910.
- Chechik G, Anderson MJ, Bar-Yosef O, Young ED, Tishby N, Nelken I (2006) Reduction of information redundancy in the ascending auditory pathway. *Neuron* 51:359–368.
- Connors BW, Prince DA (1982) Effects of local anesthetic QX-314 on the membrane properties of hippocampal pyramidal neurons. *J Pharmacol Exp Ther* 220:476–481.
- Cruikshank SJ, Rose HJ, Metherate R (2002) Auditory thalamocortical synaptic transmission *in vitro*. *J Neurophysiol* 87:361–384.
- de la Rocha J, Marchetti C, Schiff M, Reyes AD (2008) Linking the response properties of cells in auditory cortex with network architecture: cotuning versus lateral inhibition. *J Neurosci* 28:9151–9163.
- De Ribaupierre F, Goldstein MH Jr, Yeni-Komshian G (1972) Intracellular study of the cat's primary auditory cortex. *Brain Res* 48:185–204.
- de Villers-Sidani E, Simpson KL, Lu YF, Lin RC, Merzenich MM (2008) Manipulating critical period closure across different sectors of the primary auditory cortex. *Nat Neurosci* 11:957–965.
- Deisseroth K, Feng G, Majewska AK, Miesenböck G, Ting A, Schnitzer MJ (2006) Next-generation optical technologies for illuminating genetically targeted brain circuits. *J Neurosci* 26:10380–10386.
- Dominguez M, Becker S, Bruce I, Read H (2006) A spiking neuron model of cortical correlates of sensorineural hearing loss: spontaneous firing, synchrony, and tinnitus. *Neural Comput* 18:2942–2958.
- Froemke RC, Merzenich MM, Schreiner CE (2007) A synaptic memory trace for cortical receptive field plasticity. *Nature* 450:425–429.
- Gordon JA, Stryker MP (1996) Experience-dependent plasticity of binocular responses in the primary visual cortex of the mouse. *J Neurosci* 16:3274–3286.
- Hensch TK, Fagiolini M (eds.) (2004) *Excitatory-inhibitory balance: synapses, circuits, systems*. New York: Kluwer Academic/Plenum Publishing.
- Hensch TK (2005) Critical period plasticity in local cortical circuits. *Nat Rev Neurosci* 6:877–888.
- Hensch TK, Fagiolini M, Mataga N, Stryker MP, Baekkeskov S, Kash SF (1998) Local GABA circuit control of experience-dependent plasticity in developing visual cortex. *Science* 282:1504–1508.
- Hofer SB, Mrsic-Flogel TD, Bonhoeffer T, Hübener M (2006) Lifelong learning: ocular dominance plasticity in mouse visual cortex. *Curr Opin Neurobiol* 16:451–459.
- Kawai H, Lazar R, Metherate R (2007) Nicotinic control of axon excitability regulates thalamocortical transmission. *Nat Neurosci* 10:1168–1175.
- Lee CC, Sherman SM (2008) Synaptic properties of thalamic and intracortical inputs to layer 4 of the first- and higher-order cortical areas in the auditory and somatosensory systems. *J Neurophysiol* 100:317–326.
- Linden JF, Liu RC, Sahani M, Schreiner CE, Merzenich MM (2003) Spectrotemporal structure of receptive fields in areas AI and AAF of mouse auditory cortex. *J Neurophysiol* 90:2660–2675.
- Liu RC (2006) Prospective contributions of transgenic mouse models to central auditory research. *Brain Res* 1091:217–223.
- Luo L, Callaway EM, Svoboda K (2008) Genetic dissection of neural circuits. *Neuron* 57:634–660.
- MacLean JN, Fenstermaker V, Watson BO, Yuste R (2006) A visual thalamocortical slice. *Nat Methods* 3:129–134.
- Margrie TW, Brecht M, Sakmann B (2002) *In vivo*, low-resistance, whole-cell recordings from neurons in the anaesthetized and awake mammalian brain. *Pflugers Arch* 444:491–498.
- Moucha R, Kilgard MP (2006) Cortical plasticity and rehabilitation. *Prog Brain Res* 157:111–122.
- Niell CM, Stryker MP (2008) Highly selective receptive fields in mouse visual cortex. *J Neurosci* 28:7520–7536.
- Nikolenko V, Poskanzer KE, Yuste R (2007) Two-photon photostimulation and imaging of neural circuits. *Nat Methods* 4:943–950.
- Ohl FW, Scheich H (2005) Learning-induced plasticity in animal and human auditory cortex. *Curr Opin Neurobiol* 15:470–477.
- Ojima H, Murakami K (2002) Intracellular characterization of suppressive responses in supragranular pyramidal neurons of cat primary auditory cortex *in vivo*. *Cereb Cortex* 12:1079–1091.
- Oswald AM, Reyes AD (2008) Maturation of intrinsic and synaptic properties of layer 2/3 pyramidal neurons in mouse auditory cortex. *J Neurophysiol* 99:2998–3008.
- Rose HJ, Metherate R (2005) Auditory thalamocortical transmission is reliable and temporally precise. *J Neurophysiol* 94:2019–2030.
- Scholl B, Wehr M (2008) Disruption of balanced cortical excitation and inhibition by acoustic trauma. *J Neurophysiol* 100(2):646–656.
- Shen JX, Xu ZM, Yao YD (1999) Evidence for columnar organization in the auditory cortex of the mouse. *Hear Res* 137:174–177.
- Simon JZ, Depireux DA, Klein DJ, Fritz JB, Shamma SA (2007) Temporal symmetry in primary auditory cortex: implications for cortical connectivity. *Neural Comput* 19:583–638.
- Sohya K, Kameyama K, Yanagawa Y, Obata K, Tsumoto T (2007) GABAergic neurons are less selective to stimulus orientation than excitatory neurons in layer II/III of visual cortex, as revealed by *in vivo* functional Ca²⁺ imaging in transgenic mice. *J Neurosci* 27:2145–2149.
- Soto G, Kopell N, Sen K (2006) Network architecture, receptive fields, and neuromodulation: computational and functional implications of cholinergic modulation in primary auditory cortex. *J Neurophysiol* 96:2972–2983.
- Stiebler I, Neulist R, Fichtel I, Ehret G (1997) The auditory cortex of the mouse: left–right differences, tonotopic organization and quantitative analysis of frequency representation. *J Comp Physiol A* 181:559–571.

- Sutter ML, Schreiner CE, McLean M, O'Connor KN, Loftus WC (1999) Organization of inhibitory frequency receptive fields in cat primary auditory cortex. *J Neurophysiol* 82:2358–2371.
- Tallal P, Gaab N (2006) Dynamic auditory processing, musical experience and language development. *Trends Neurosci* 29:382–390.
- Tan AY, Atencio CA, Polley DB, Merzenich MM, Schreiner CE (2007) Unbalanced synaptic inhibition can create intensity-tuned auditory cortex neurons. *Neuroscience* 146:449–462.
- Tan ML, Borst JG (2007) Comparison of responses of neurons in the mouse inferior colliculus to current injections, tones of different durations, and sinusoidal amplitude-modulated tones. *J Neurophysiol* 98:454–466.
- Verbny YI, Erdélyi F, Szabó G, Banks MI (2006) Properties of a population of GABAergic cells in murine auditory cortex weakly excited by thalamic stimulation. *J Neurophysiol* 96:3194–3208.
- Volkov IO, Galazjuk AV (1991) Formation of spike response to sound tones in cat auditory cortex neurons: interaction of excitatory and inhibitory effects. *Neuroscience* 43:307–321.
- Wang XJ (2008) Decision making in recurrent neuronal circuits. *Neuron* 60:215–234.
- Watts J, Thomson AM (2005) Excitatory and inhibitory connections show selectivity in the neocortex. *J Physiol* 562:89–97.
- Wehr M, Zador AM (2003) Balanced inhibition underlies tuning and sharpens spike timing in auditory cortex. *Nature* 426:442–446.
- Weinberger NM (2004) Specific long-term memory traces in primary auditory cortex. *Nat Rev Neurosci* 5:279–290.
- Wu GK, Arbuckle R, Liu BH, Tao HW, Zhang LI (2008) Lateral sharpening of cortical frequency tuning by approximately balanced inhibition. *Neuron* 58:132–143.
- Yan J, Zhang Y (2005) Sound-guided shaping of the receptive field in the mouse auditory cortex by basal forebrain activation. *Eur J Neurosci* 21:563–576.
- Zhang LI, Bao S, Merzenich MM (2001) Persistent and specific influences of early acoustic environments on primary auditory cortex. *Nat Neurosci* 4:1123–1130.
- Zhang LI, Tan AY, Schreiner CE, Merzenich MM (2003) Topography and synaptic shaping of direction selectivity in primary auditory cortex. *Nature* 424:201–205.

(Accepted 15 July 2009)